VELOCITY-SPACE RING-PLASMA INSTABILITY, MAGNETIZED

PART I: THEORY

by

J.K. Lee and C.K. Birdsall

Memorandum No. UCB/ERL M78/38

28 June 1978

ELECTRONICS RESEARCH LABORATORY

College of Engineering
University of California, Berkeley
94720

TABLE of CONTENTS

ABSTRACT

The interaction of magnetized monoenergetic ions (a ring in velocity space) with a homogeneous Maxwellian target plasma is studied numerically using the linear Vlasov theory. The ring may be produced when an energetic beam is injected perpendicularly to a uniform magnetic field. In addition to the previously known results, we find that this flute-like instability may be classified into three distinct regimes based on the "beam" density relative to the plasma density, where many features such as physical mechanisms, dispersion diagrams, and maximum growth rates are quite different. The effects of electron dynamics, plasma or ring thermal spread, the ratio of ω_p/ω_c for plasma ions, and electromagnetic modifications are also considered. Most of the theoretical results of Part I are closely verified by simulations, presented in Part II.

I. INTRODUCTION

A beam-plasma-like instability occurs when the "beam" is a ring in velocity space at speed v_b with the ring thermal spread, $v_{tr} \lesssim v_b$ and the plasma is cool, $v_{tp} \lesssim v_b$, for $\underline{k} \perp \underline{B}_o$ (cf. Fig. 1). The unmagnetized ring-plasma was studied extensively by Mynick *et al.* (1977). The magnetized ring-plasma was studied by Tataronis and Crawford (1970). This paper, Part I, extends the magnetized ring-plasma linear theory and Part II presents particle-fluid simulations verifying the linear theory as well as presenting nonlinear behavior.

A neutral beam injected perpendicularly to a uniform magnetic field ($\underline{B}_o$) into a target plasma becomes ionized and forms an energetic charged ring in the velocity-space perpendicular to $\underline{B}_o$. The interaction of this beam (now a ring) with a homogeneous Maxwellian target plasma drives a flute-like ($k_\parallel = 0$) velocity-space instability. Recent laboratory experiments [Seiler *et al.* (1976), Seiler (1977), Yamada *et al.* (1977), Böhmer (1976)] confirm this instability.

We examine the magnetized cold ring-warm plasma interaction through the linear (i.e., small amplitude) Vlasov theory and computer simulations, both for electrostatic and for electromagnetic cases.

We also examine the magnetized warm ring-warm plasma case through linear Vlasov theory.

For the electrostatic case, our study includes interactions among two species (ring ions and plasma ions) and among three species (ring ions, plasma ions and plasma electrons). The results are valid for ring speed much less than Alfven speed. For $v_b \gtrsim v_A$, the electro-

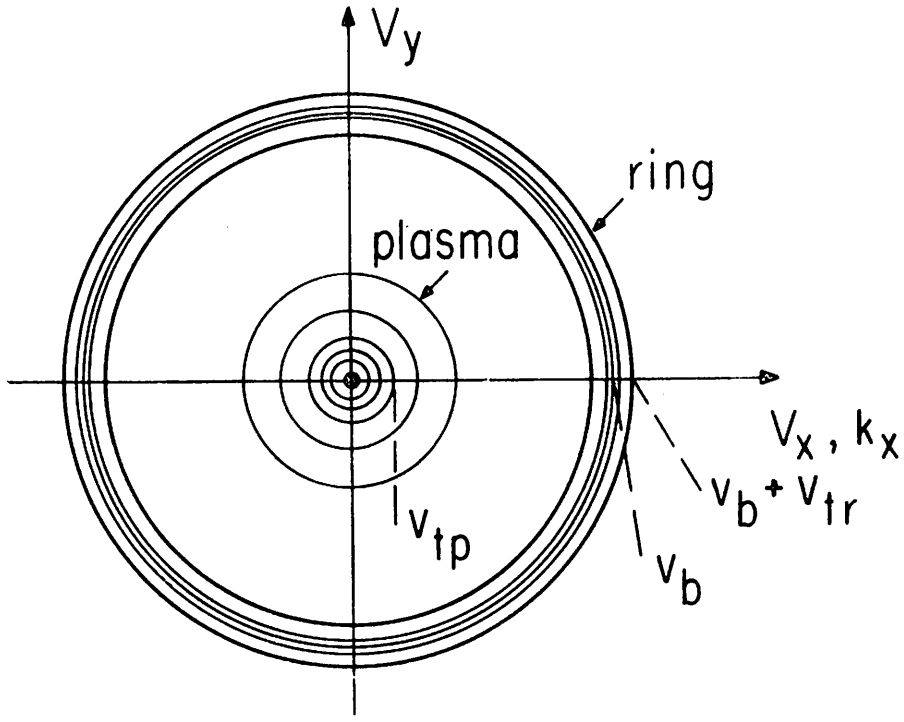

Fig. 1 The density distribution of the two-component homogeneous plasma in the velocity-space perpendicular to a uniform magnetic field ($\underline{B} = B_o\hat{z}$). The low speed component (called "plasma") is a Maxwellian with thermal spread v_{tp} ; the energetic component (called "ring") has a relatively high mean speed v_b with thermal spread v_{tr} . The wave vector is in the x-direction perpendicular to $B_o\hat{z}$.

magnetic case, only the three species interactions are considered with the plasma electrons cold. In the theory and in simulations, the target plasma is assumed to be Maxwellian in velocity, homogeneous in space, infinite, and linear; it is treated as a set of collisionless particles in the linear Vlasov theory and as a collisionless linear fluid in the hybrid simulations. We look for modes growing in time for real wave vectors ($\underline{k}$) perpendicular to $\underline{B}_o$.

Parameters are chosen close to those for a mirror fusion experiment, which we will call our prototype model, such as

$$\left(\frac{\omega_{ppi}}{\omega_{ci}}\right)^2 \approx 1000$$

$$\frac{v_b}{v_{tp}} \approx 13$$

and the ring density relative to the plasma density,

$$R \equiv \frac{n_b}{n_p} = \left(\frac{\omega_{pbi}}{\omega_{ppi}}\right)^2$$

varying from 5×10^{-4} to ≈ 1 . Here, ω_{ppi} and ω_{pbi} are the plasma frequencies of the target plasma ions and the beam ions, respectively. ω_{ci} is the ion cyclotron frequency of the ring ions (or of the target plasma ions; these two are the same since identical ion species, like deuterium ring-deuterium plasma, are considered), v_b is the perpendicular speed ($v_\perp$) of the ring ions, and v_{tp} is the perpendicular thermal spread of the Maxwellian target plasma ions. These parameters correspond approximately to 100 keV deuterium beam and 1 keV deuterium plasma of $n_p \approx 10^{14}$ cm^{-3} in a 60 kilogauss magnetic field.

We know from the linear theory of Vlasov-Poisson equations that this velocity-space ring-plasma combination sets up an absolute instability of relatively large growth rates ($\sim\omega_{ci}$) [Tataronis and Crawford (1970)]. In addition, we find three distinct regimes for the density ranges of our interest.

For a *weak ring*, with $5\times10^{-4} \lesssim R \lesssim 5\times10^{-3}$, the maximum growth rate is $\gamma/\omega_{ci} \lesssim 1$ and rises as $R^{0.6}$; for most of this regime the ring-plasma instability is due to the coupling between some ring Bernstein harmonics and the plasma lower hybrid wave, and is like that observed in the laboratory by Seiler *et al.* (1976, 1977), who had a smaller value of ω_{ppi}/ω_{ci}. However, their analytical model differs from ours in the use of the unmagnetized ring-magnetized plasma model compared to our magnetized ring-magnetized plasma model.

In the *intermediate ring* case, with $5\times10^{-3} \lesssim R \lesssim 5\times10^{-2}$, γ/ω_{ci} is $\gtrsim 1$, and goes as $R^{0.35}$, and the most unstable mode is not the same as in the weak ring regime, but an enhanced Dory-Guest-Harris mode [Dory *et al.* (1965)].

For a *strong ring*, with $5\times10^{-2} \lesssim R \lesssim 1.0$, the growth rate is further increased and varies as $R^{0.17}$; here the most unstable mode is an ion acoustic-type mode excited by the ring-plasma combination even without the presence of electrons (i.e., the role of the electron Debye shielding is carried by the hot and strong ring ion component), which exists even when the uniform magnetic field is turned off.

This mode is similar to that studied by Mynick *et al.* (1977) and Hall and Heckrotte (1965).

We have made electrostatic and electromagnetic simulations over the above ranges of ring density and observed the predicted linear behavior (i.e., the growth rates and frequencies of the growing modes) remarkably closely, using a linearized fluid model for the plasma and (fully nonlinear) particles for the ring. These results appear in Part II, following. In addition the nonlinear evolution is studied in great detail.

The remainder of this paper summarizes the linear Vlasov theory with its detailed numerical results, which enable the classification of this instability into several beam density regimes. Various parameter effects as well as electromagnetic effects are also discussed.

II. ELECTROSTATIC DISPERSION RELATION

Our two-species velocity-space-ring-plasma system is neutral ($n_{oi} = n_{oe}$) and has uniform density and magnetic field (B_o). The plasma (or target) has a Maxwellian ion velocity distribution of thermal spread v_{tp} with density n_p. The ion ring (or beam) has mean speed v_b ($v_b \gg v_{tp}$) with density, $n_b = Rn_p$. Electrons form a uniform neutralizing background and are otherwise ignored. The generalization to three-species (thus including plasma electron dynamics) or to electromagnetic cases will be considered later in this part.

The linear theory leading to the dispersion relation for this electrostatic two-species system has been developed by many authors. The results of Tataronis and Crawford (1970) will be summarized below, followed by extensive numerical results with their interpretation.

The linearized Vlasov-Poisson Equations are

$$\nabla^2\phi(\underline{r},t) = -\sum_s \frac{q_s}{\epsilon_o}\int d\underline{v}\, f_{1s}(\underline{r},\underline{v},t) \tag{1}$$

$$\frac{\partial f_{1s}}{\partial t}(\underline{r},\underline{v},t) + \underline{v}\cdot\nabla f_{1s}(\underline{r},\underline{v},t) + \frac{q_s}{m_s}\underline{v}\times B_o\cdot\frac{\partial f_{1s}}{\partial \underline{v}}(\underline{r},\underline{v},t)$$

$$= \frac{q_s}{m_s}\nabla\phi(\underline{r},t)\cdot\frac{\partial f_{os}}{\partial \underline{v}}(\underline{r},\underline{v}) \ . \tag{2}$$

Here ϕ is the perturbed field potential; q_s and m_s are the charge and the mass of each species (ring ions or plasma ions); f_{1s} is the

lowest order perturbed velocity distribution, and f_{os} is the unperturbed velocity distribution of each species, which takes the following form after being integrated over the parallel (to $\underline{B}_o$) component of velocities

$$f_b(v_\perp) = (2\pi v_b)^{-1}\ \delta(v_\perp - v_b) \tag{3}$$

$$f_p(v_\perp) = (2\pi v^2_{tp})^{-1}\ \exp\ (-v_\perp^2/2v^2_{tp}). \tag{4}$$

Then, for $k_\parallel = 0$, the electrostatic dispersion relation becomes

$$1 = \frac{\omega^2_{ppi}}{\omega^2_{ci}} \sum_{\ell=-\infty}^{\infty} \frac{e^{-\lambda} I_\ell(\lambda)}{\lambda} \frac{\ell\omega_{ci}}{\omega - \ell\omega_{ci}} + \frac{\omega^2_{pbi}}{\omega^2_{ci}} \sum_{\ell=-\infty}^{\infty} \frac{1}{\mu_\perp} \frac{dJ^2_\ell(\mu_\perp)}{d\mu_\perp} \frac{\ell\omega_{ci}}{\omega - \ell\omega_{ci}} \tag{5}$$

where

$$\lambda \equiv \left(\frac{k_\perp v_{tp}}{\omega_{ci}}\right)^2, \qquad \mu_\perp \equiv \frac{k_\perp v_b}{\omega_{ci}},$$

and $J_\ell(x)$ and $I_\ell(x)$ are Bessel functions of the first kind of order ℓ, of real and imaginary arguments, respectively.

These equations are solved numerically using the dispersion equation solving code, ROOTS [Gerver (1976)].

III. CLASSIFICATION OF REGIMES BY RING DENSITY

In obtaining the numerical results of the linear Vlasov theory, we fixed the following parameters, varying only the ring relative density (R) unless otherwise specified

$$\frac{\omega_{ppi}}{\omega_{ci}} \approx 32$$

$$\frac{v_b}{v_{tp}} = 13$$

$$\frac{v_{tr}}{v_b} = 0 \quad \text{(where } v_{tr} \text{ is the ring thermal spread)}$$

$$\frac{v_A}{v_b} = \infty \quad \text{(where } v_A \equiv B_o/(\mu_o n_i m_i)^{\frac{1}{2}} \text{ is the Alfven speed;}$$

$$n_i = n_b + n_p\text{)}.$$

Variations from the prototype parameters will be made in the next two sections.

Maximum growth rates (γ_{max}/ω_{ci}) as a function of R are plotted in Fig. 2, clearly showing three distinct regimes in the density region of our interest.

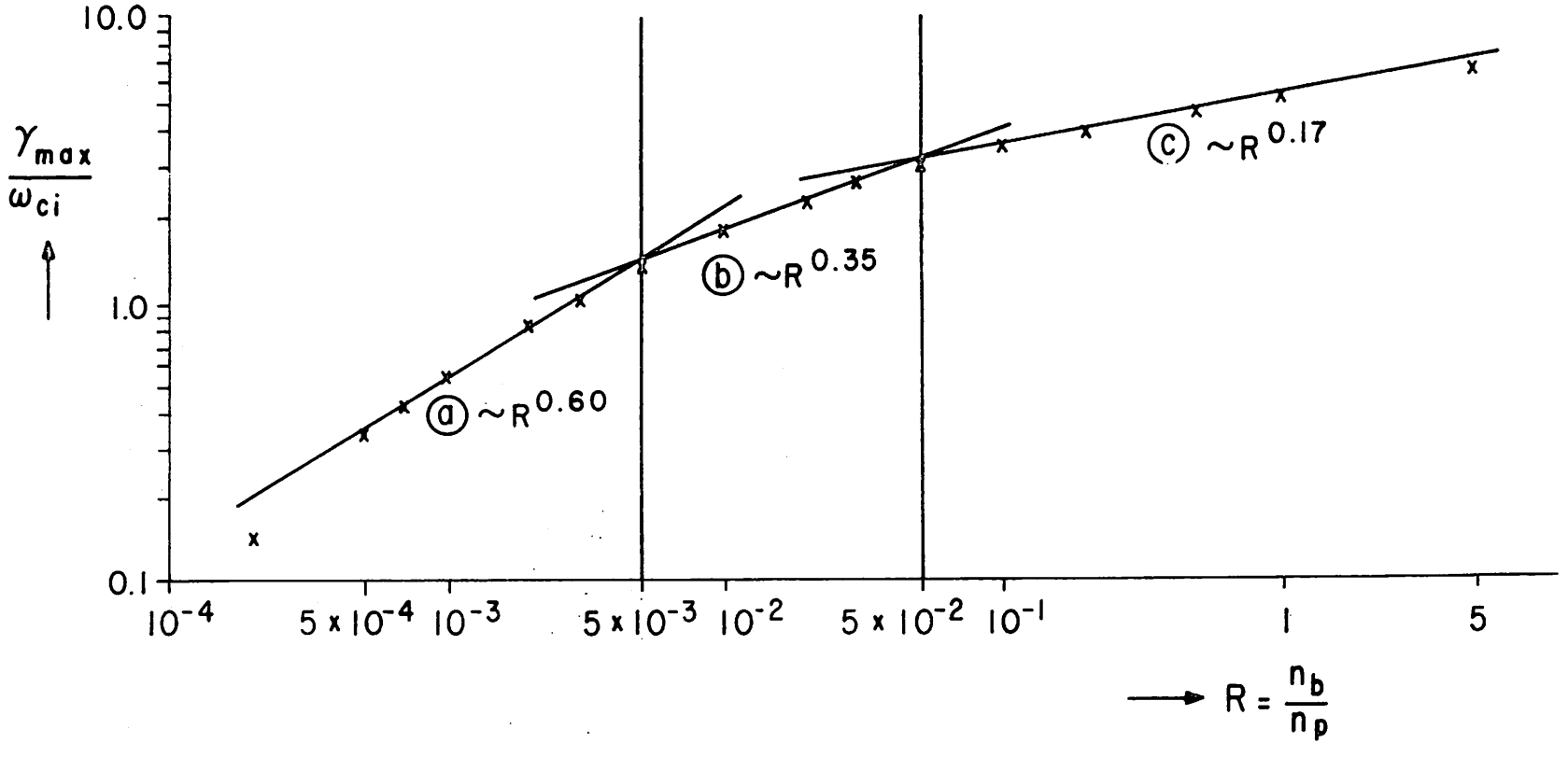

Fig. 2 Maximum growth rates normalized to the ion cyclotron frequency of ring particles versus ring-plasma density ratio ($R = n_b/n_p$). Here, $(\omega_{ppi}/\omega_{ci})^2 = 1023$, $v_b/v_{tp} = 13$; electrons are not included, and the case is wholly electrostatic. Only R is varied. The straight line fits indicate the power dependencies shown in various regimes for γ_{max}/ω_{ci}.

(1) *Weak Ring Regime* $(5 \times 10^{-4} \lesssim R \lesssim 5 \times 10^{-3})$

In this regime $\frac{\gamma_{max}}{\omega_{ci}}$ goes as $R^{0.60}$ as shown in Fig. 2, and the growth rates are smaller than the cyclotron frequency of the ring ions. Figure 3 shows that the growth regions are very discrete in wave number k with almost no overlapping. The ring-plasma instability here is due to the coupling between ring Bernstein harmonics (resonance number, $\ell \approx 32$) and the lower hybrid wave (LH). We interpret this interaction as flow of free energy which originates from the large difference in the initial velocity distributions of ring and plasma to the excitation of a collective mode, namely, the lower hybrid wave, which can occur only in the slow wave side (i.e., the phase velocity of these coupled modes are to be smaller than the ring perpendicular speed v_b).

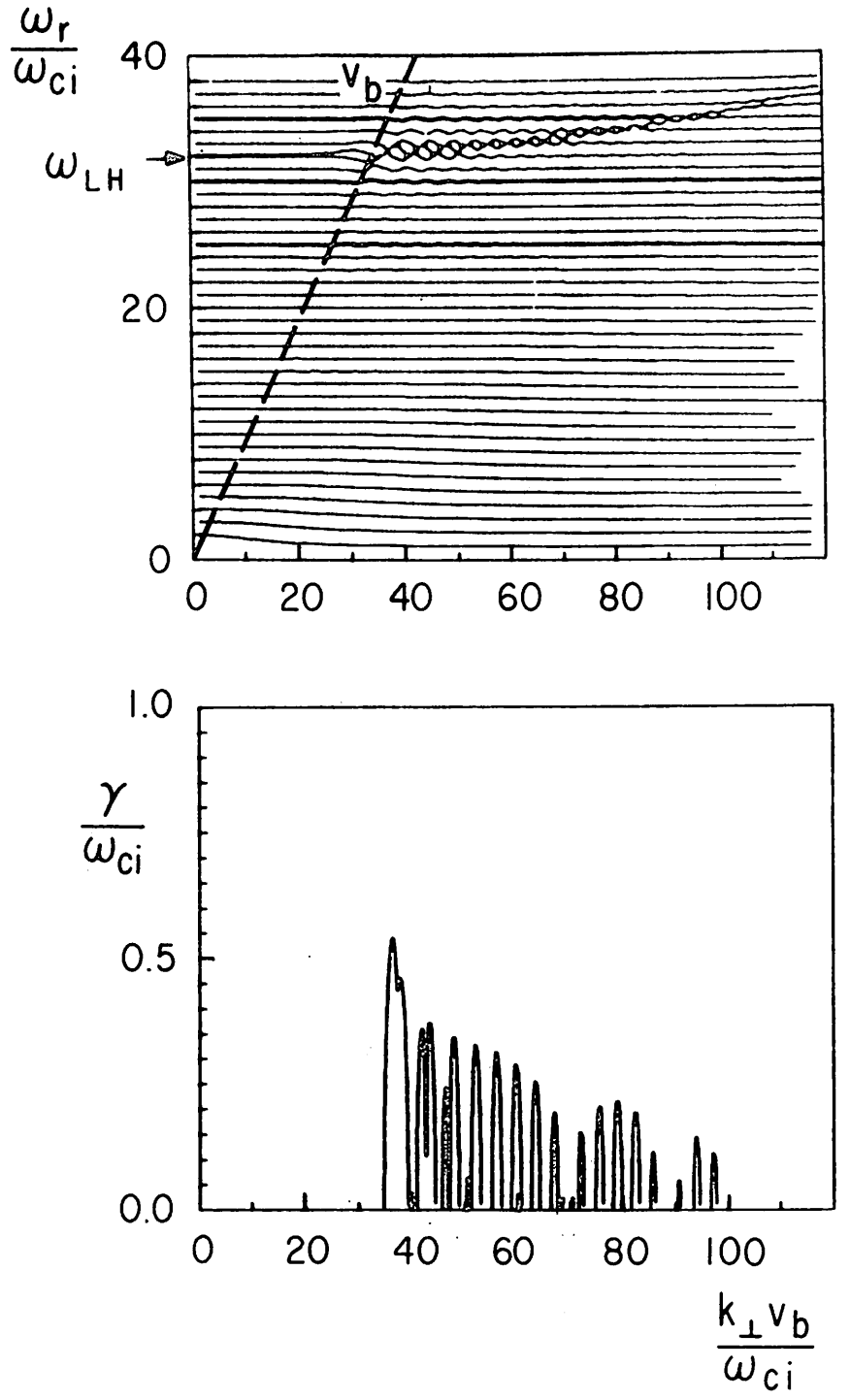

Fig. 3 Frequencies and growth rates for $R = 10^{-3}$ weak beam. $\omega_{ppi}/\omega_{ci} \approx 32$, $v_b/v_{tp} \approx 13$ with no electron dynamics (electrostatic).

(2) *Intermediate Ring Regime* $(5 \times 10^{-3} \lesssim R \lesssim 5 \times 10^{-2})$

Here $\frac{\gamma_{max}}{\omega_{ci}} \sim R^{0.35}$. The growth regions are shown in Fig. 4, with considerably larger growth rates and very little discrete structure near γ_{max} . For this ring density, the lower hybrid wave does *not* couple with the ring Bernstein harmonics as Fig. 4 shows. The dominant instability source is the ring itself, like that of Dory-Guest-Harris (DGH) modes [Dory *et al.* (1965)]. However, γ_{max} is much larger than that of a cold ring by itself, because $\frac{\gamma_{max}}{\omega_{ci}} \approx 0.5$ for the DGH instability with the similar parameter but without the plasma component. This enhancement due to the presence of the plasma component was also noted by Tataronis and Crawford (1970).

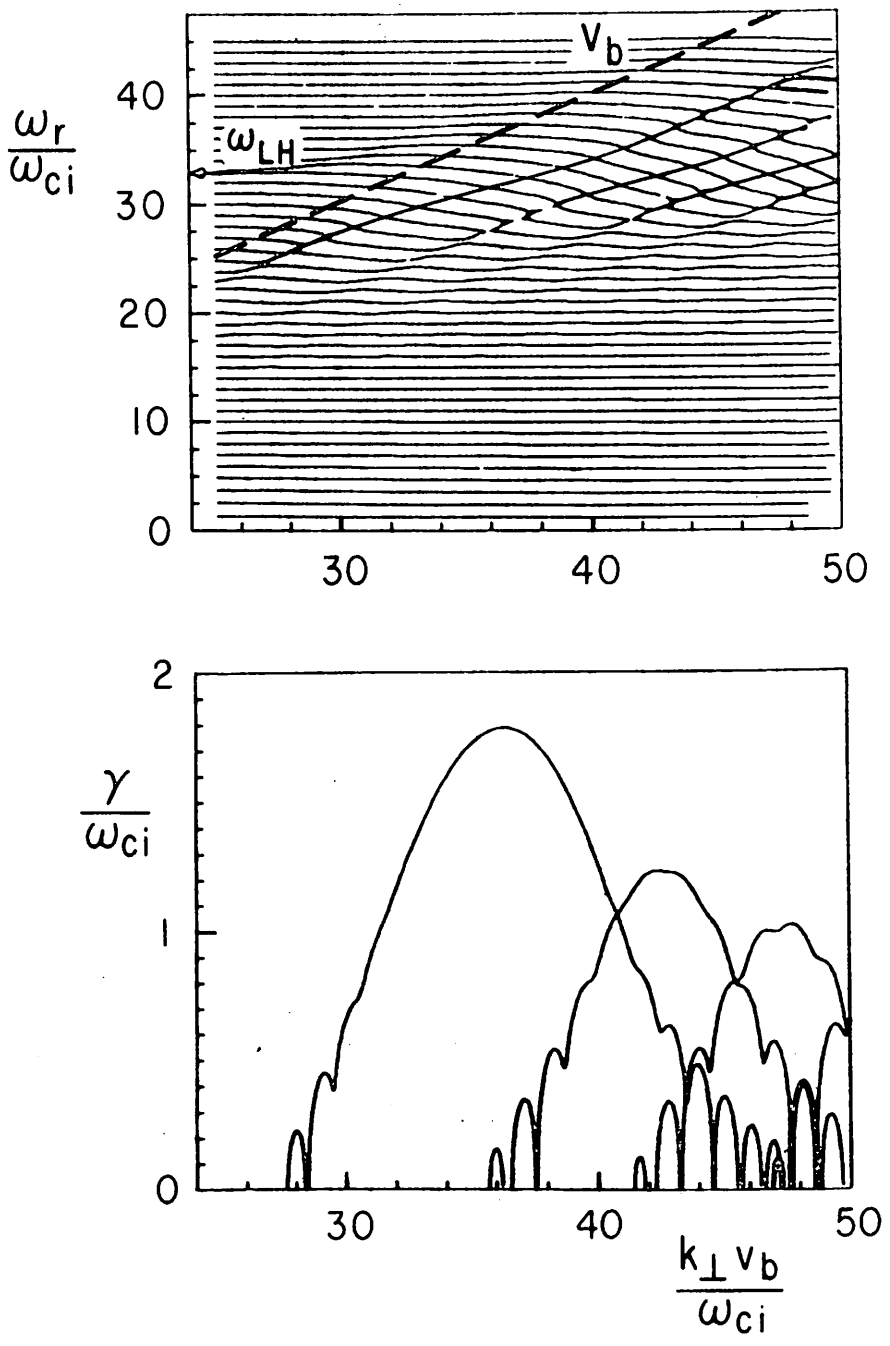

Fig. 4 Dispersion curves for $R = 10^{-2}$ intermediate beam. $\omega_{ppi}/\omega_{ci} \approx 32$, $v_b/v_{tp} \approx 13$ with no electron dynamics (electrostatic).

(3) *Strong Ring Regime* $(5 \times 10^{-2} \lesssim R \lesssim 5)$

Here $\frac{\gamma_{max}}{\omega_{ci}} \sim R^{0.17}$. The maximum growth rates are about several times larger than the ring ion cyclotron frequency. Hence, the straight line orbit approximation should hold; indirect evidence of this is the continuous variation (as against discrete) of γ vs k in Fig. 5. As in the intermediate regime, the lower hybrid wave does not couple with ring Bernstein harmonics. This is because the relatively large ring density enhances the lower hybrid frequency from 32 ω_{ci} to about 45 ω_{ci} (off the top of Fig. 5). Figure 5 also shows that several enhanced DGH modes with $\frac{\gamma_{max}}{\omega_{ci}} \approx 2$ exist but the most unstable mode has $\frac{\gamma_{max}}{\omega_{ci}} \approx 5$. The physical mechanism for the ring-plasma instability in this regime is mostly governed by the excitation of a perpendicularly propagating ion-acoustic-type mode even in the absence of electron dynamics. This mode might be called a hot-ion-shielded ion acoustic mode similar to the Mynick-Gerver-Birdsall mode [Mynick *et al.* (1977)]. With straight line orbits and cold plasma approximations, the dispersion relation becomes

$$1 = \frac{\omega_{ppi}^2}{\omega^2} + \frac{\omega_{pbi}^2}{\omega^2}\left(1 - k_\perp^2 \frac{v_b^2}{\omega^2}\right)^{-3/2} \qquad (6)$$

like that of Hall and Heckrotte (1965) and Mikhailovskii and Pashitskii (1966). This dispersion equation describes a mode whose phase velocity starts at the ring speed at small wavenumbers and roughly asymptotes to the plasma frequency of the target plasma at large wavenumbers, not disappearing even when the magnetic field is reduced

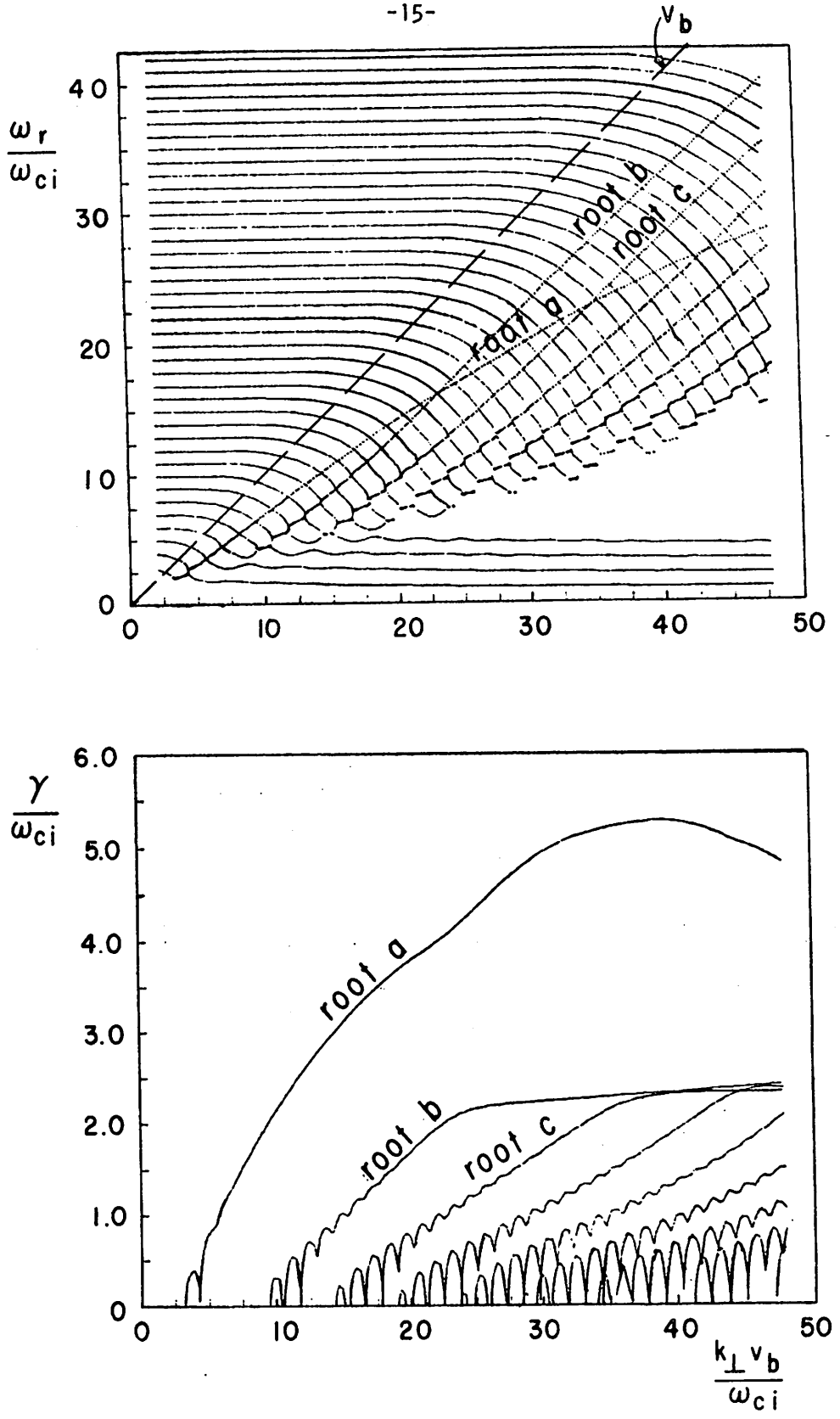

Fig. 5 Electrostatic dispersion curves for R = 1.0 strong beam, $\omega_{ppi}/\omega_{ci} \approx 32$, $v_b/v_{tp} \approx 13$, with no electron dynamics (root a survives as $\underline{B}_o \to 0$, roots b , c do not; proved by Gerver (1976)).

to zero. A plot of Eq. (6), which is not shown, is very similar to the most unstable mode appearing in Fig. 5. Our results from the dispersion equation solver for $0.25 \lesssim R \lesssim 5$ compare rather closely with those of Hall and Heckrotte (1965) (cf., their Figs. 3-4 for γ_{max} vs R and $\mathrm{Re}\,\omega$ (and $k_\perp v_b$) at the maximum growth rate vs R). This agreement is expected because Eq. (6) becomes a better approximation as the ring density increases.

The classification into three regimes in the density range of Fig. 2, which are the direct results of the linear Vlasov theory, and verified later by simulations (cf. Part II), can also be expected by the following qualitative arguments. The first boundary separating the weak and the intermediate regimes is roughly consistent with the onset of the DGH instability [Dory *et al.* (1965)] due to the ring alone. As R increases with $\frac{\omega_{ppi}}{\omega_{ci}} \approx 32$ fixed, $\frac{\omega_{pbi}}{\omega_{ci}}$ increases to reach the threshold value ($\approx \sqrt{6}$) of the DGH instability; thus, below this threshold density (i.e., in the weak ring regime) there is no DGH mode, and above it (in the intermediate and the strong ring regimes) DGH modes exist. The fact that DGH modes in the ring-plasma instability are affected by the presence of the target plasma component, which does not exist in the pure DGH instability, makes the onset density in the ring-plasma instability ($R \approx 5 \times 10^{-3}$) slightly different from that of the pure DGH instability ($R \approx 6 \times 10^{-3}$).

The second boundary between the intermediate and the strong regimes is consistent with the threshold for a straight line orbit approximation, which occurs when $\frac{\gamma}{\omega_{ci}} \approx (k_\perp v_b / 4\omega_{ci})^{\frac{1}{2}}$, namely, when a resonant ion stays in phase with the wave for at least a growth time

($\sim\gamma^{-1}$) [Mynick *et al.* (1977), and Lindgren *et al.* (1976)]. The parameter in Fig. 5 provides $(k_\perp v_b/4\omega_{ci})^{\frac{1}{2}} \approx 3.0$, which corresponds to $R \tilde{\approx} 4\times 10^{-2}$ in Fig. 2. Thus, it roughly agrees with $R \approx 5\times 10^{-2}$ of the Vlasov theory (and simulation); thus, below this boundary (in the intermediate range) DGH modes are the only unstable modes, but above this threshold (in the strong ring regime) DGH modes are dominated by the new mode provided by the straight line orbit approximation.

In addition, classification via ring density is also found to hold for saturation levels. The simulations shown in Part II also have three distinct regimes whose boundaries are similar to those in the classification via growth rates (see Fig. 2).

IV. EFFECTS of VARYING PARAMETERS

So far only the prototype model has been considered, namely, with the two equal species (deuterium ring and deuterium plasma where electrons form a massless neutralizing background), $\frac{v_b}{v_{tp}} = 13$, $\frac{v_{tr}}{v_b} = 0$, $\frac{v_A}{v_b} = \infty$ and $\frac{\omega_{ppi}}{\omega_{ci}} \approx 32$. In the following we consider the effects of variation from the prototype model; it will be understood that the electrostatic prototype model parameters are used unless otherwise noted.

(1) *Adding Electron Dynamics*

From solving the electrostatic dispersion equation with the electron polarization drift term, $\left(\frac{\omega_{ppe}}{\omega_{ce}}\right)^2$, included with the vacuum term of Eq. (5), we find that adding cold electrons to the target plasma simply reduces real frequencies and growth rates slightly, with the results qualitatively unchanged. Figure 6, with electrons, shows little change from Fig. 3, without electrons. Adding electrons with perpendicular speed equal to that of ring ions, in addition to the cold plasma electrons, provided a dispersion diagram identical to that of the three-species case (i.e., ring ions, plasma ions, and cold plasma electrons). This is expected because of the small electron gyroradius ($k_\perp \rho_e << 1$) and the large electron gyrofrequency. The top two curves in Fig. 7 compare the cases with and without electron dynamics.

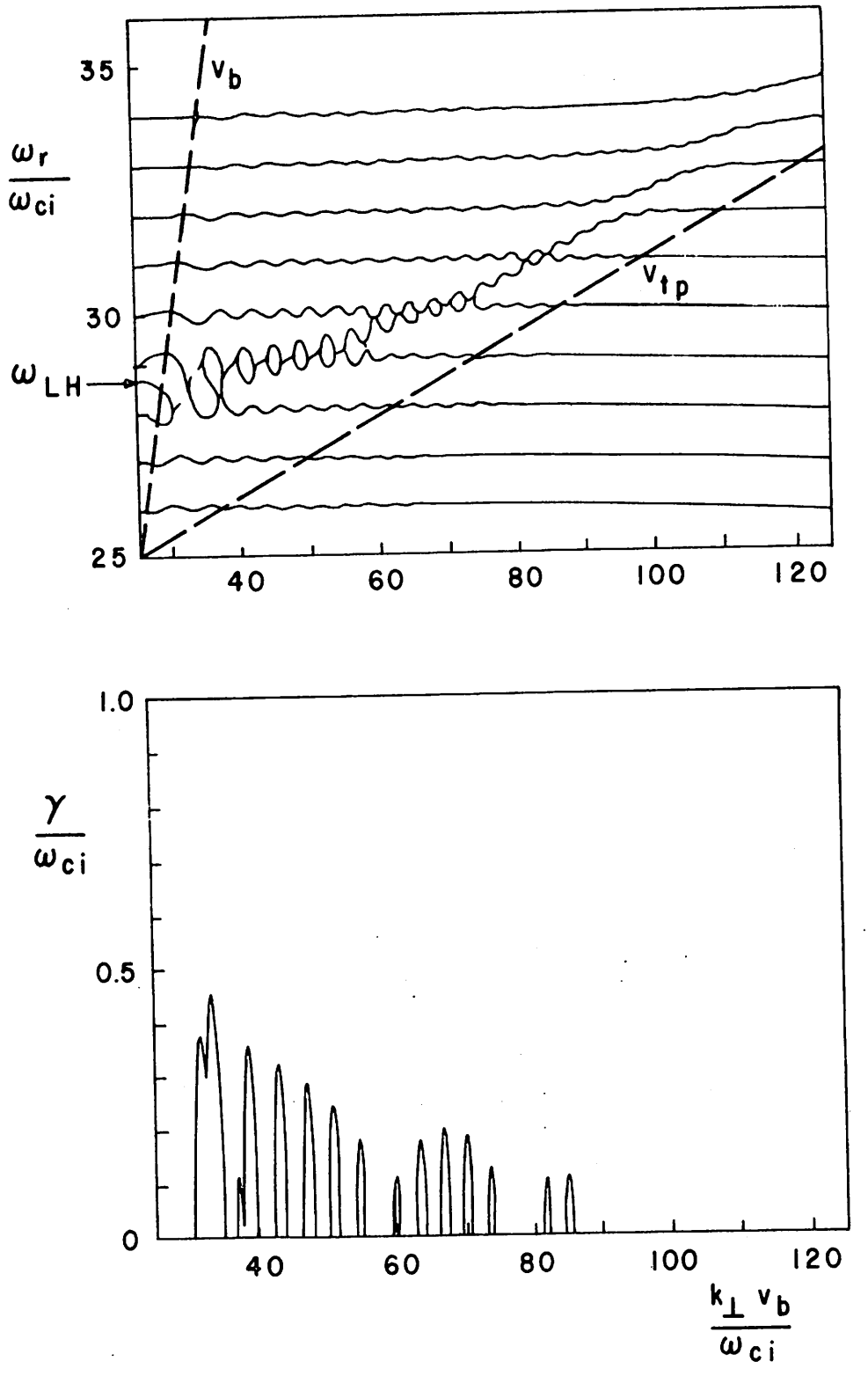

Fig. 6 Electrostatic dispersion curves with cold plasma electrons included (of mass ratio, $m_e/m_i = 1/3700$). As in Fig. 3, $R = 10^{-3}$, $\omega_{ppi}/\omega_{ci} \approx 32$, $v_b/v_{tp} \approx 13$. Note that frequencies and growth rates drop slightly, and the new lower hybrid (LH) frequency is

$$\omega_{LH} = \left[\frac{\omega_{ppi}^2}{1 + (\omega_{ppe}/\omega_{ce})^2} + \omega_{ci}^2 \right]^{\frac{1}{2}} \approx 28.3\ \omega_{ci}$$

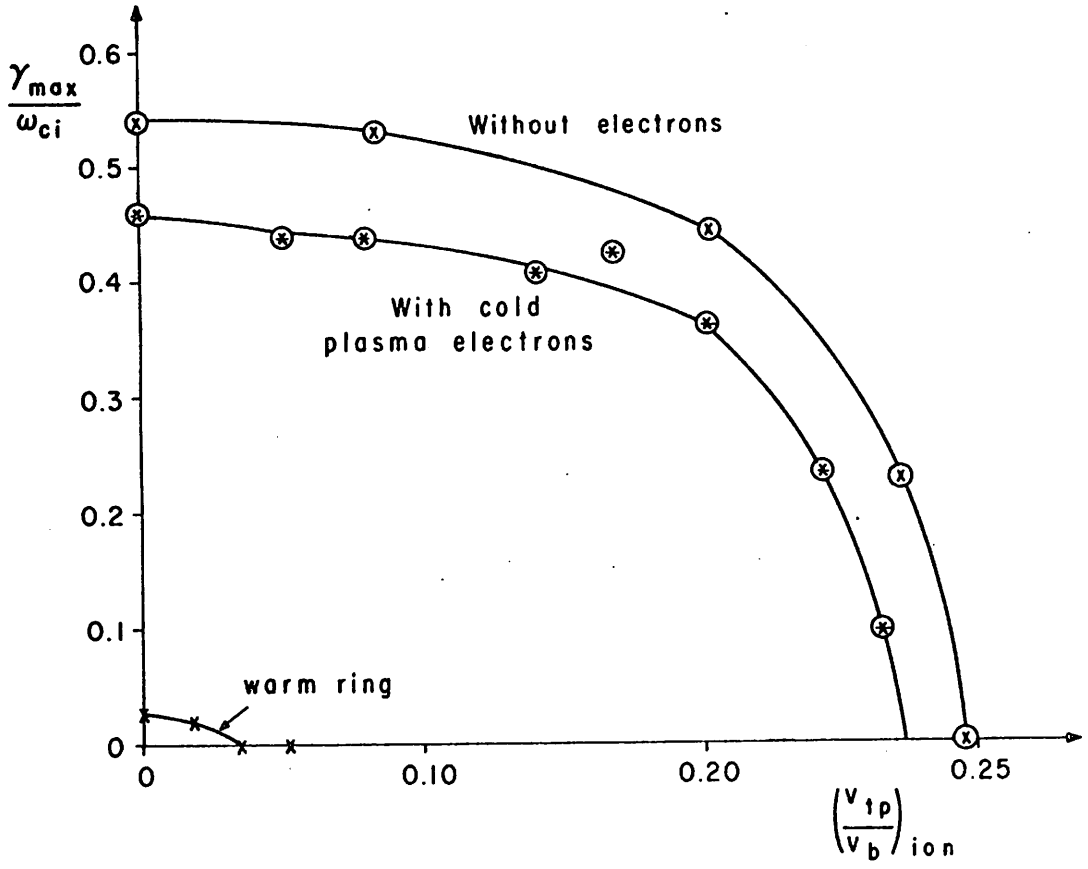

Fig. 7 Effects of electrons and of the plasma thermal spread for a weak ring case ($R = 10^{-3}$) where $\omega_{ppi}/\omega_{ci} \approx 32$; $v_A/v_b = \infty$, $m_e/m_i = 1/3700$ (when electrons are used in the center curve); $v_{tr}/v_b = 0$ for the top two curves, and about 0.5 for the bottom warm ring case. Curves connect the points obtained from solving the dispersion relation.

(2) *Stabilizing Effects of the Plasma Thermal Spread*

The variation of the parameter $\frac{v_{tp}}{v_b}$ is considered in Fig. 7 for the two- and the three-species cases in a weak ring regime ($R = 10^{-3}$). Note that the end of growth at $\frac{v_{tp}}{v_b} \approx 0.25$ for this magnetized cold ring model is about half the value (≈ 0.45) found by Mynick *et al.* (1977) for the unmagnetized cold ring. Also plotted here is the effect of the plasma thermal spread using a warm ring distribution with $\frac{v_{tr}}{v_b} \approx 0.5$ fixed. The warm ring is modeled by subtracting two Maxwellians with equal peak densities (the ratios of the squared thermal velocities of these two Maxwellians is defined as the mirror ratio, which is 1.1 in this case).

An intermediate ring case ($R = 10^{-2}$) is considered in Fig. 8 for two models: a cold ring and a warm ring. Again, the plasma thermal spread needed for no instability of a cold ring is about half that by Mynick *et al.* (1977).

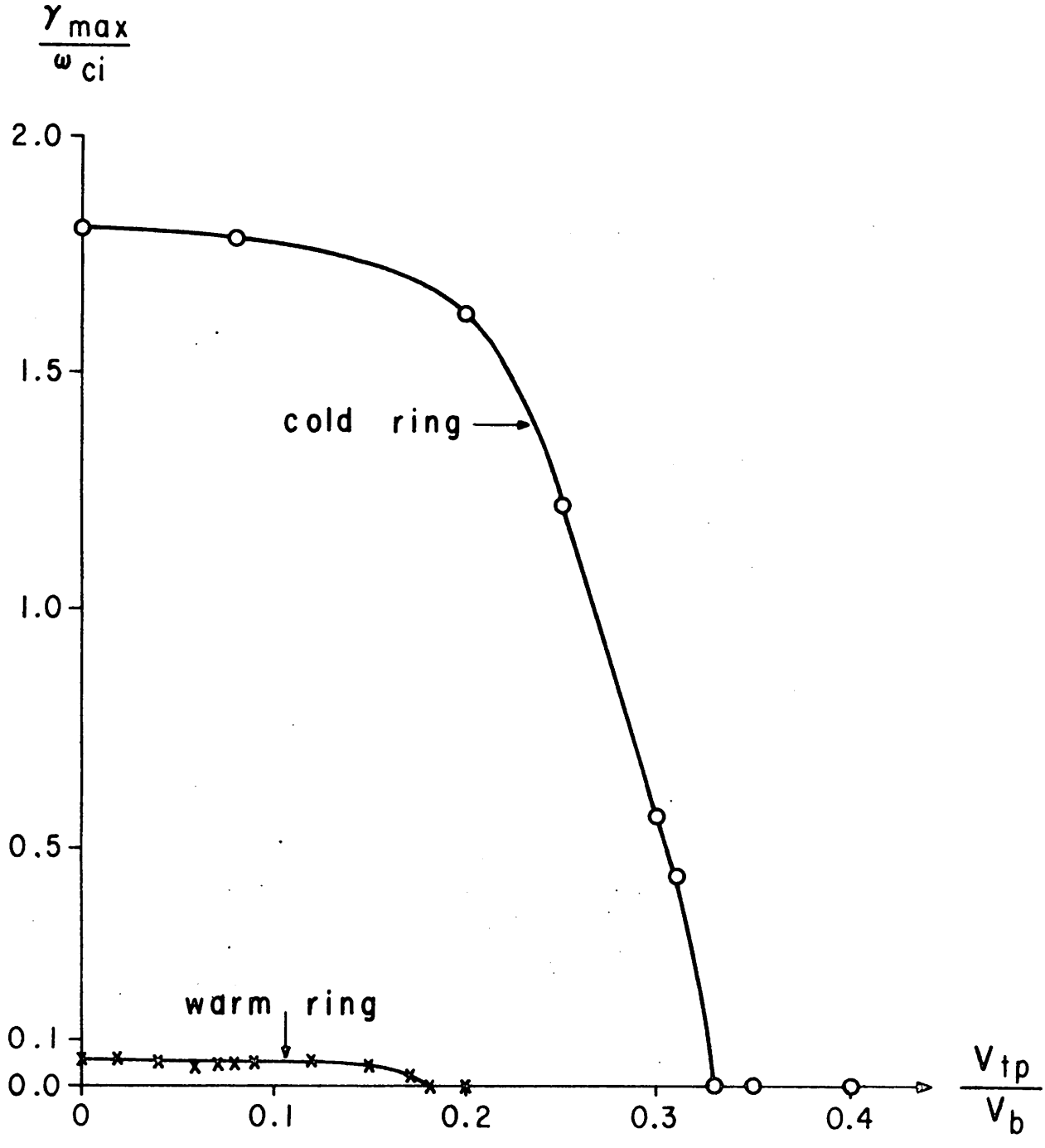

Fig. 8 An intermediate ring case ($R = 10^{-2}$): the effects of the thermal spreads of the plasma and of the ring. Here, $\omega_{ppi}/\omega_{ci} \approx 32$, $v_A/v_b = \infty$, $m_e/m_i = 0$; $v_{tr}/v_b = 0$ for the top curve (cold ring case) and about 0.5 for the bottom curve (warm ring case).

(3) *Stabilizing Effects of the Ring Thermal Spread*

(a) *Magnetized Case*

As the ring thermal spread increases, the coupling characteristics change from fluid coupling to resonant kinetic coupling [cf. O'Neil and Malmberg (1968); Seiler (1977)]. A warm ring with $\frac{v_{tr}}{v_b} \approx 0.5$, which is well above the required beam thermal spread for the transition from the beam-type (fluid coupling) to the Landau-type (resonant kinetic coupling) picture, is examined for two cases of the ring densities ($R=10^{-3}$ and 10^{-2}) in Figs. 7-8. Due to the resonant characteristics, the growth rate is very dependent on the frequency mismatch for a warm ring case with $R=10^{-2}$, shown in Fig. 9; the roots from the dispersion equation with varying frequency mismatches, agree very nicely with other theoretical predictions of a resonant coupling with a mismatch, which give a circle:

$$\frac{\gamma_{max}}{\omega_{ci}} = \left[\left(\frac{\gamma_o}{\omega_{ci}}\right)^2 - \left(\frac{\Delta\omega}{2}\right)^2\right]^{\frac{1}{2}} .$$

Here, $\Delta\omega \equiv (\omega_{ppi} - \ell\omega_{ci})/\omega_{ci}$ with $\ell = 32$, and γ_o/ω_{ci} is the peak maximum growth rate at zero mismatch. In contrast, where the ring is cold (where $v_{tr}/v_b = 0$ with other parameters the same) there is very little effect of frequency mismatch (no real change in γ_{max} as $\Delta\omega$ changes since $\gamma_{max}/\omega_{ci} = 1.792$ at $\Delta\omega/2 = -0.055$, 1.798 at $\Delta\omega/2 = -0.008$, and 1.813 at $\Delta\omega/2 = 0.125$). In this case the lower hybrid wave couples with the Bernstein harmonics (thus beam-type unstable modes). This coupling is in contrast to the warm ring case where the Bernstein harmonics involved in resonant kinetic coupling are from the plasma rather than from the ring due to the greatly broadened ring

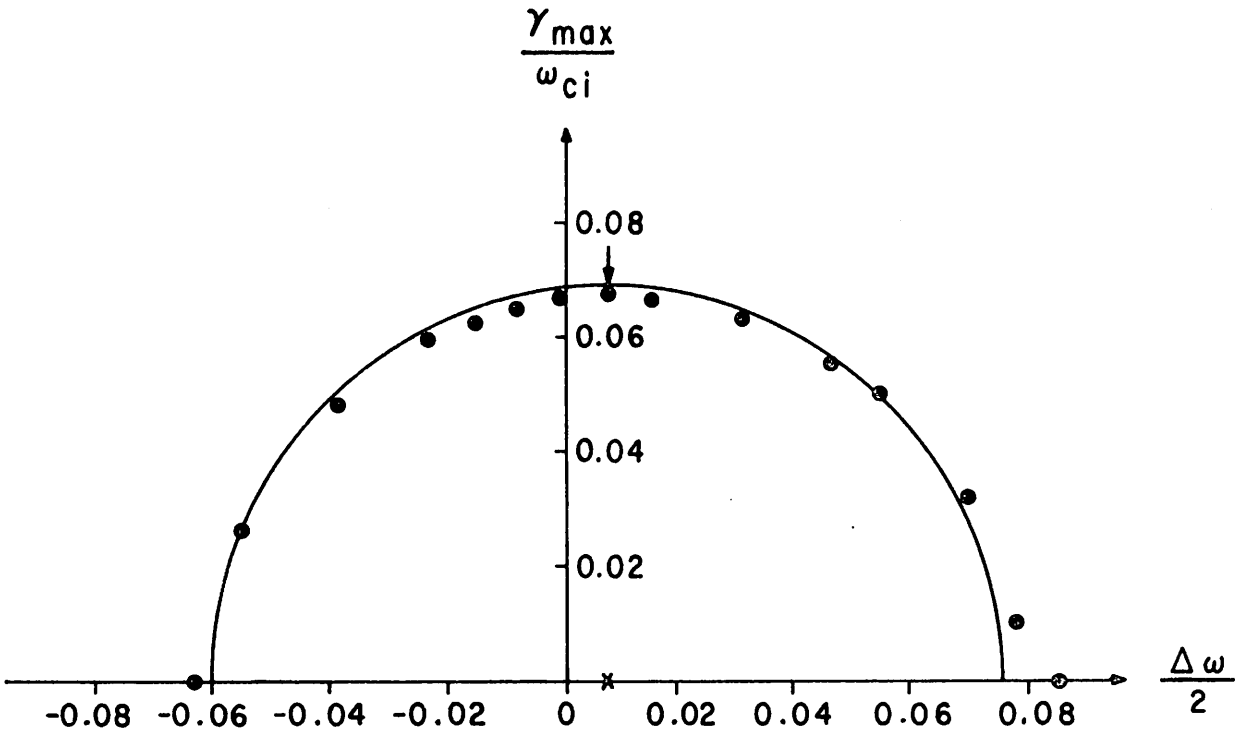

Fig. 9 The effects of frequency mismatches ($\Delta\omega$) for a warm ring ($v_{tr}/v_b \approx 0.5$) with $R = 10^{-2}$, $v_{tp}/v_b = 0$, $v_A/v_b = \infty$, $m_e/m_i = 0$. The roots from the dispersion solver (marked as dots) form a circle with the radius given by the peak growth rate (indicated with an arrow); the center of the circle is at $\Delta\omega/2 = 0.08$ (marked x), slightly shifted from the expected value.

velocity distribution. Thus, the frequency mismatch between the plasma Bernstein harmonics and the plasma frequency of the plasma component (or this could be some type of a hybrid wave) is an important factor for the resonant kinetic coupling.

(b) *Unmagnetized Case*

The variation of v_{tr}/v_b is summarized in Fig. 10 for the unmagnetized model, namely, using the straight line orbit approximation, which provides only qualitative information. The warm ring distribution for an unmagnetized model is modeled by a shifted Maxwellian (different from the previous loss cone type warm ring)

$$f_b(v_\perp) \sim \exp\left[-2\frac{(v_\perp - v_b)^2}{jv_b^2}\right] ,$$

so that the parameter j determines the thermal spread of the warm ring v_{tr}/v_b . This figure shows that, as expected, the maximum growth rate decreases as the ring thermal spread is increased and that the complete stabilization occurs when the initial ring thermal spread is about 20% of the ring mean speed.

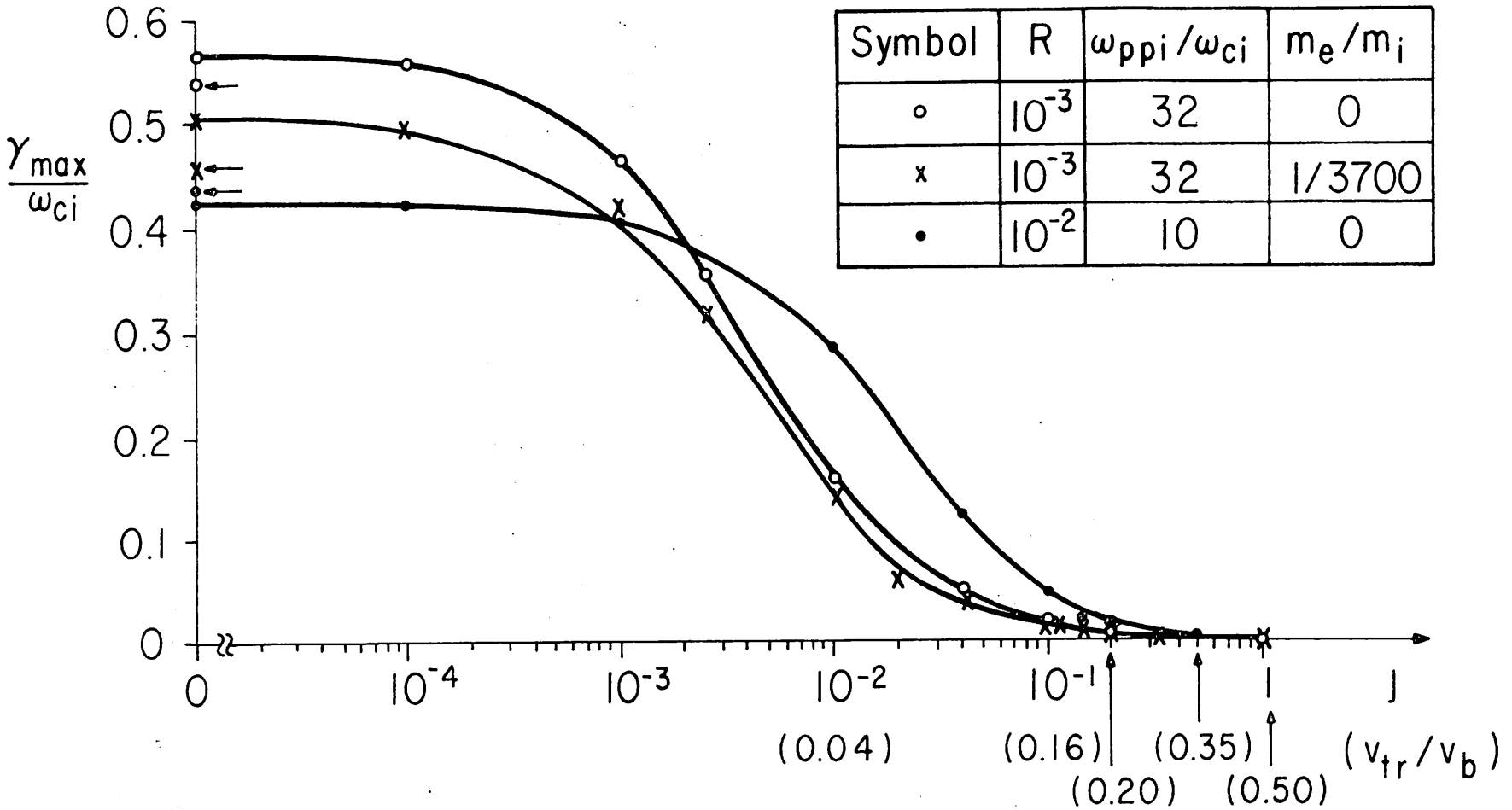

Fig. 10 The stabilization effects of the ring thermal spreads for three different cases using the straight line orbit approximation. The other common parameters not in the legend are $v_b/v_{tp} = 13$, $v_A/v_b = \infty$ (wholly electrostatic). For zero ring thermal spreads (thus delta function-like distributions) the magnetized results are shown with arrows in the left side of the figure.

(4) *Effects of the Target Plasma Density*

The variation of γ_{max}/ω_{ci} with ω_{ppi}/ω_{ci} is shown in Fig. 11 both for the magnetized and for the unmagnetized models with $R = 10^{-3}$. As the target plasma becomes denser, the maximum growth rate increases for a fixed ring-to-plasma density ratio and the discrepancy between the magnetized and the unmagnetized models becomes smaller. Both results are expected because the threshold of unstable DGH modes and that of the straight line orbit approximation are exceeded as ω_{ppi}/ω_{ci} increases.

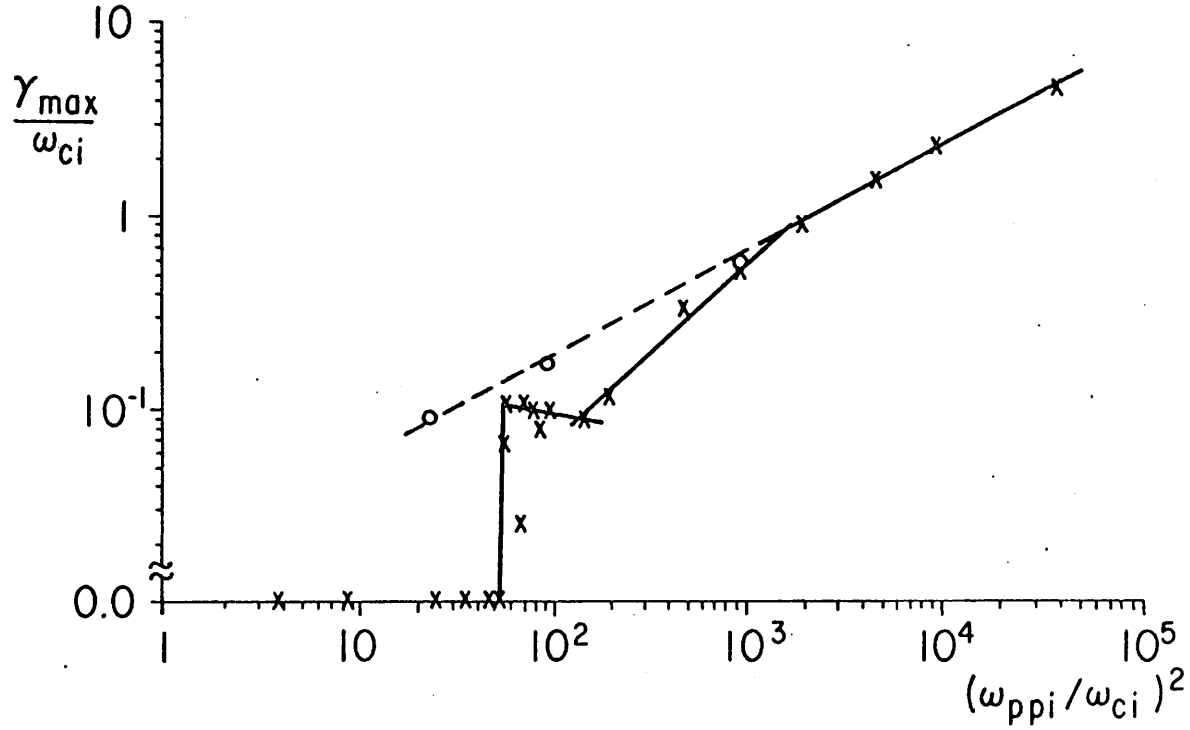

Fig. 11 Effects of the target plasma density for the delta function ring with $R = 10^{-3}$, $v_b/v_{tp} = 13$, $v_A/v_b = \infty$ and $m_e/m_i = 0$. Results of the magnetized model are marked x, and those of the unmagnetized marked 0. It is observed that even with $R = 10^{-3}$, unstable DGH modes start to appear from $(\omega_{ppi}/\omega_{ci})^2 \approx 5000$.

(5) *Effects of Unlike Ion Species*

So far for simplicity only the deuterium-deuterium interaction has been considered. The electrostatic dispersion diagram in Fig. 12 for the cold deuterium ring and tritium plasma (without electron dynamics) with, $R = 10^{-3}$, provides a pattern similar to Fig. 3 where the plasma Bernstein harmonics appear as unaffected straight lines in between the wiggled ring Bernstein harmonics due to smaller cyclotron frequency; hence the lower hybrid couples with the Bernstein harmonics of the ring ions rather than with those of the plasma ions in the weak ring regime.

Also the dispersion (not shown here) of the cold deuterium ring and the warm deuterium plasma with a slightly differing ion mass ratio shows that Bernstein harmonics of the plasma are straight lines while ring Bernstein harmonics are curved lines leading also to the above conclusion on which Bernstein harmonics are involved in the lower hybrid coupling for a cold ring case.

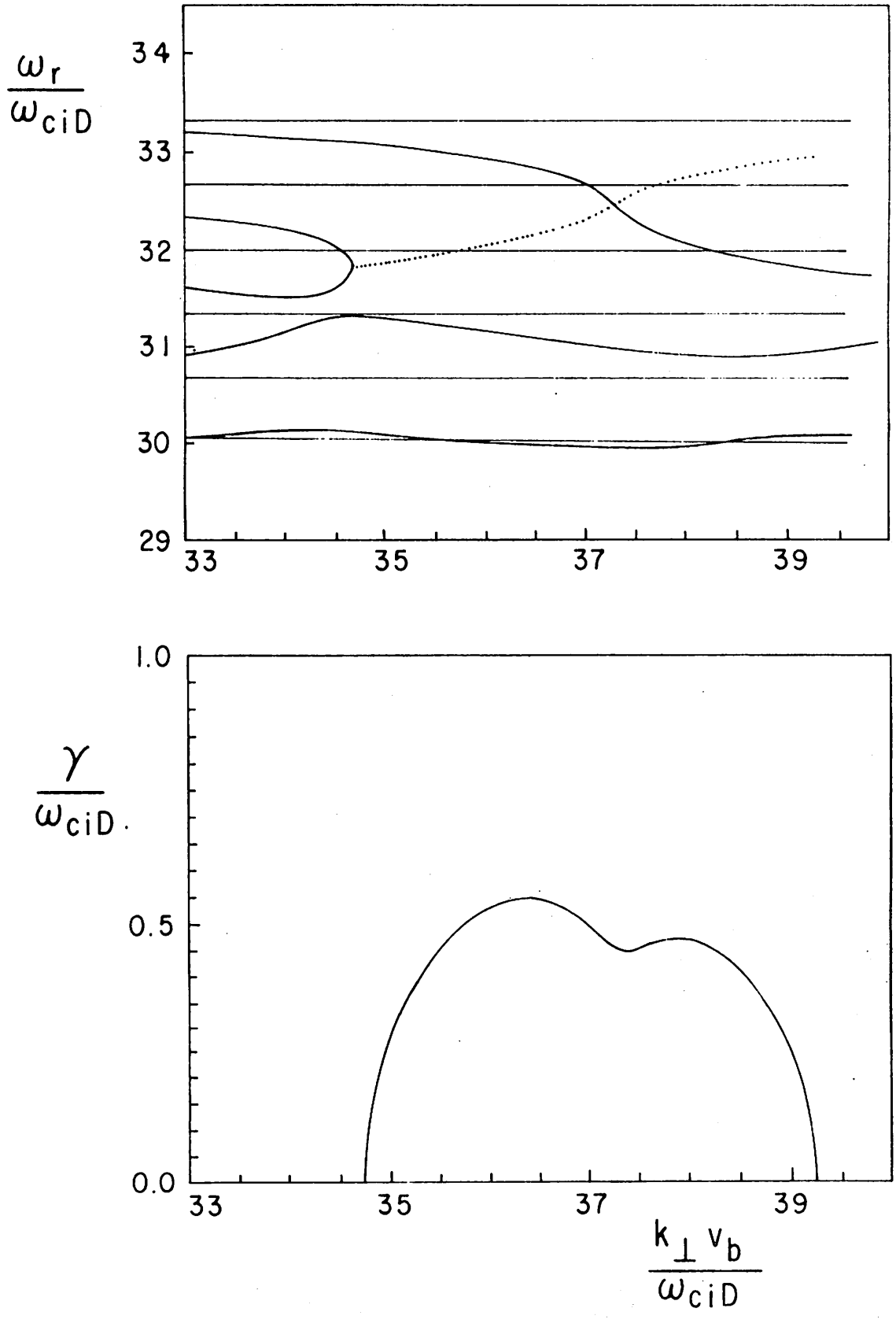

Fig. 12 The electrostatic dispersion of cold deuterium ring and warm tritium plasma with no electron dynamics; $R = 10^{-3}$, $\omega_{ppi}/\omega_{ci} \approx 32$, $v_b/v_{tp} = 13$ and $m_D/m_T = 2/3$ (thus $\omega_{ciD} = 1$, $\omega_{ciT} = 0.667$) . There are two kinds of Bernstein harmonics, those of the ring ions (curved lines with spacing ≈ 1 in the normalized frequency unit) and of the plasma ions (straight lines with spacing $= 0.667$).

V. ELECTROMAGNETIC MODIFICATION

To consider electromagnetic effects we adopt the ordering scheme of electromagnetic modification terms in the dispersion tensor of Callen and Guest (1971, 1973) to obtain the following simplified (still approximate) electromagnetic dispersion relation including the electron polarization drift term $\omega_{ppe}^2/\omega_{ce}^2$ and the $\underline{E}_1 \times \underline{B}_o$ drift term of electrons $(\omega_{ppe}^2/\omega_{ce}^2)(\omega_{ppe}^2/c^2k^2)$

$$1 + \left(\frac{\omega_{ppe}}{\omega_{ce}}\right)^2 \left(1 + \frac{\omega_{ppe}^2}{c^2k^2}\right) = \frac{\omega_{ppi}^2}{\omega_{ci}^2} \sum_{\ell=-\infty}^{\infty} \frac{e^{-\lambda} I_\ell(\lambda)}{\lambda} \frac{\ell\omega_{ci}}{\omega - \ell\omega_{ci}}$$

$$+ \frac{\omega_{pbi}^2}{\omega_{ci}^2} \sum_{\ell=-\infty}^{\infty} \frac{1}{\mu_\perp} \frac{dJ_\ell^2(\mu_\perp)}{d\mu_\perp} \frac{\ell\omega_{ci}}{\omega - \ell\omega_{ci}} \quad . \quad (7)$$

This equation was solved by the dispersion solver, ROOTS [Gerver (1976)] with some modification. As the indicator of electromagnetic effects, the ratio of the beam perpendicular speed v_b to the Alfven speed v_A will be used.

For $R = 10^{-3}$, two electromagnetic cases are shown here. Figure 13 is a modestly electromagnetic case since the slope v_A of the magnetosonic (MS) branch is still larger than v_b, so that the MS branch does not couple with ring Bernstein harmonics; the instability is due to the coupling between ring Bernstein harmonics and the lower hybrid (LH) branch at the slow wave side (i.e., $\omega/k < v_b$) as in the electrostatic cases. Figure 14 shows a strongly electromagnetic case where v_A is smaller

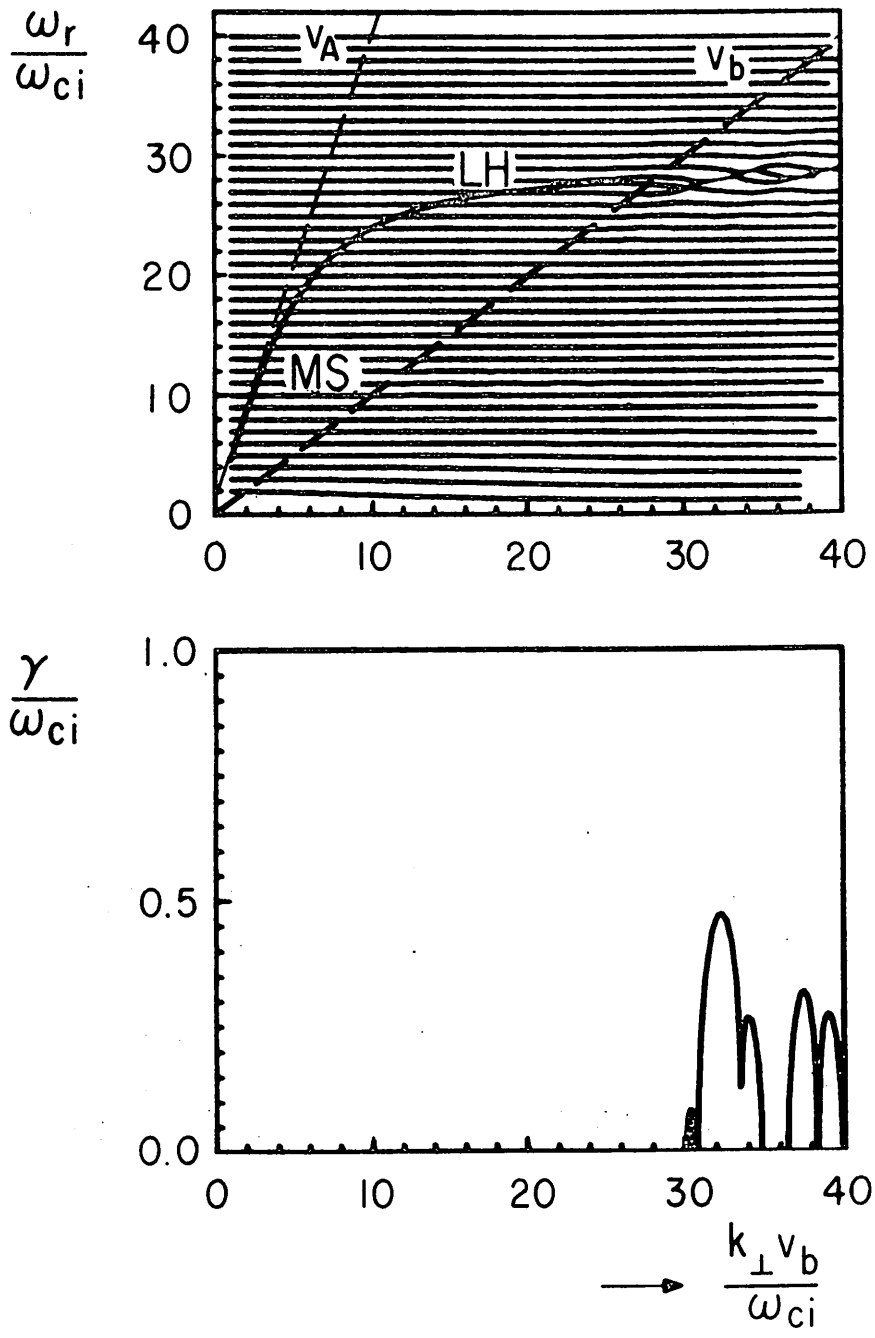

Fig. 13 Three-species electromagnetic dispersion with cold plasma electrons of mass ratio, $m_e/m_i = 1/3700$. As in Figs. 3 and 6, $R = 10^{-3}$, $\omega_{ppi}/\omega_{ci} \approx 32$, $v_b/v_{tp} \approx 13$, but $v_b/v_A \approx 0.23$.

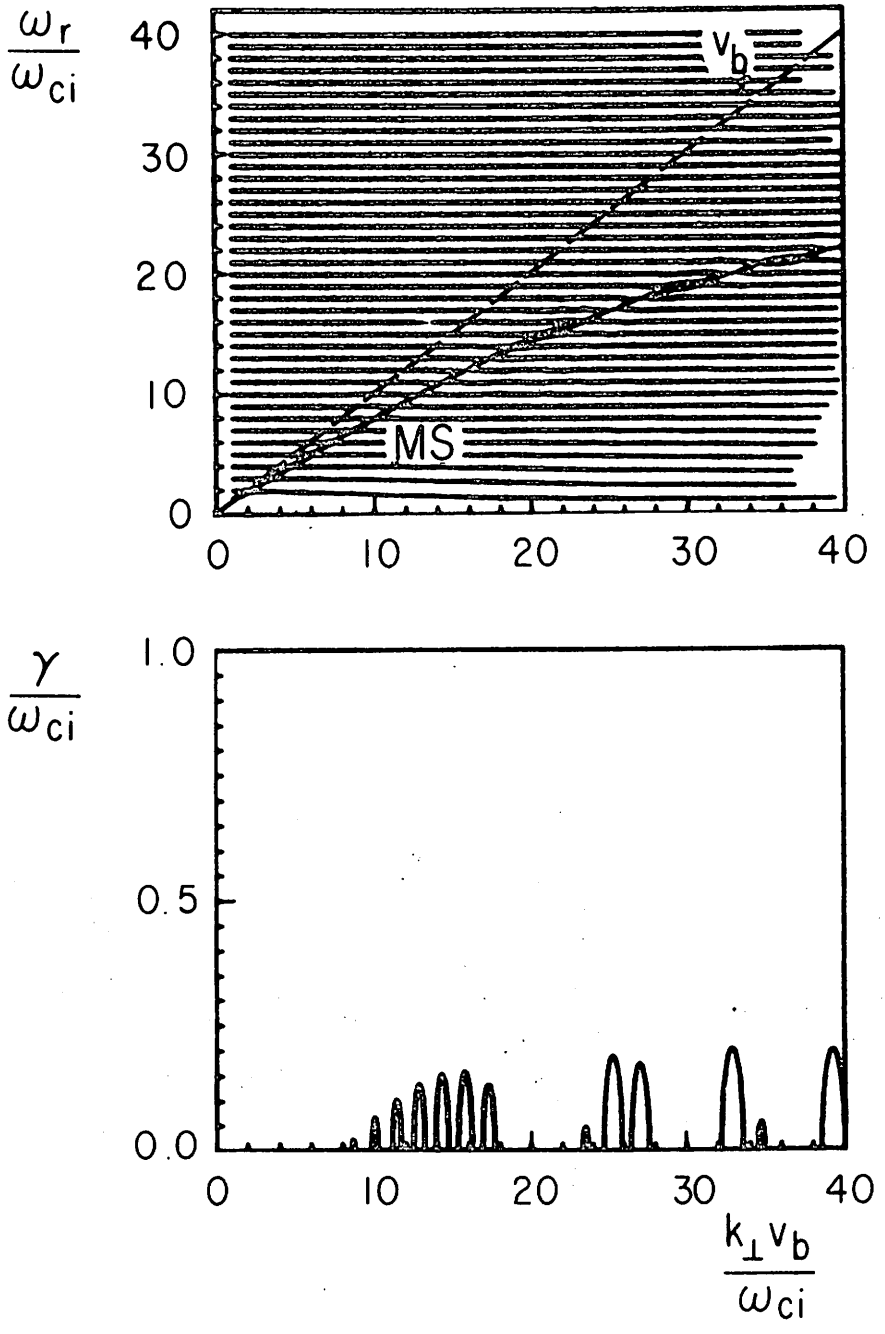

Fig. 14 Same as in Fig. 13 except that $v_b/v_A \approx 1.3$.

than v_b , so that the MS branch can couple with ring Bernstein harmonics. The real frequencies as well as the growth rates of the growing modes are gradually lowered as electromagnetic effects become more important. This is expected since the added electromagnetic terms make the left hand side of Eq. (7) larger than that in the electrostatic case, giving a stabilizing effect to the ring-plasma instability. These electromagnetic effects are summarized in Fig. 15 for various values of R and v_b/v_A .

Symbol	R	$\frac{m_i}{m_e}$	$\left(\frac{\omega_{ppi}}{\omega_{ci}}\right)^2$
◇	.1	400	1000
∘	.01	400	1000
X	.01	100	1000
△	.01	400	100
○	.001	3704	1000

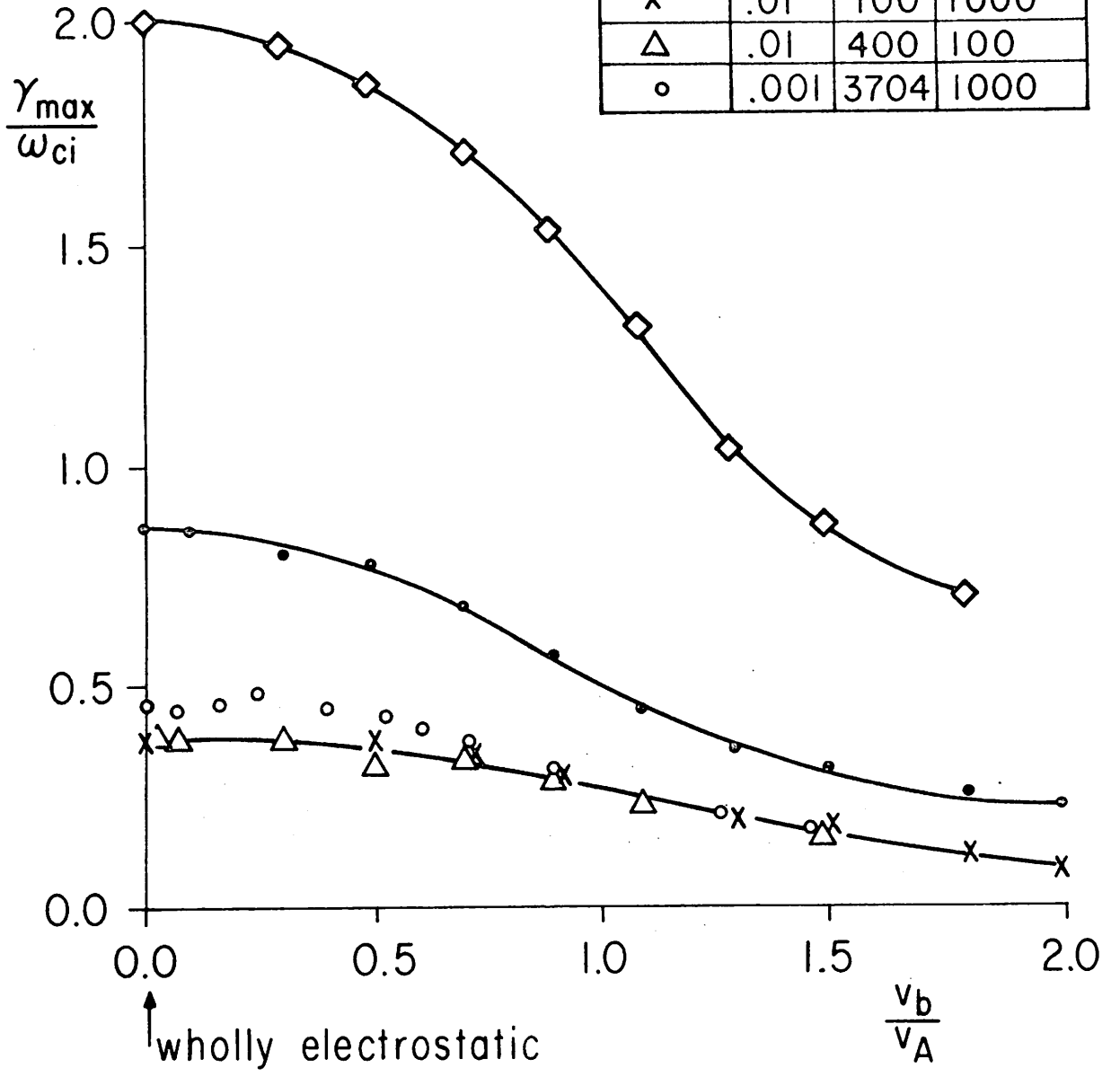

Fig. 15 Electromagnetic stabilization. v_A is decreased as the electromagnetic effect is increased with $v_b / v_{tp} \approx 13$ fixed. Curves are drawn just to connect these theoretical points. Figures 13-14 correspond to selective cases of symbol 0.

VI. CONCLUSIONS

This paper extended the study of the linear Vlasov theory for a magnetized ring-plasma instability by solving the linear dispersion relation numerically for various choices of parameters.

We found from these results that the instability may be classified into several different regimes according to the ratio of the ring density relative to the plasma density. In each regime, the physical mechanisms for the instability differ from one another, thus yielding different dispersion spectra as well as different maximum growth rates (from $0.3\ \omega_{ci}$ to $\sim 10\ \omega_{ci}$). The nonlinear phenomenon such as saturation levels in simulations (in Part II) also reveals similar classification.

Electrons are found to play a relatively unimportant but slightly stabilizing role in this ion-ion instability. Increasing the thermal spread of the plasma or of the ring component also stabilizes the instability. The effects of the plasma density were also considered with $(\omega_{pi}/\omega_{ci})^2$ varying from the low density range (~ 1) to the 2X11B range ($\sim 10^5$).

The electromagnetic effects on this instability were considered by including a simple modification term [à la Callen and Guest (1971, 1973)] to the electrostatic dispersion relation. An appreciably reduced ($\sim \frac{1}{2}$) maximum growth rate is expected when the Alfven speed is comparable to the beam mean speed.

Most of these theoretical results have been verified very closely by computer simulations, which appear in Part II.

ACKNOWLEDGMENTS

We would like to express our appreciation to Michael Gerver for his useful dispersion equation solver ROOTS.

This work was supported by the U.S. Department of Energy Contract EY-76-S-03-0034-PA128.

REFERENCES

1965 Dory, R. A., Guest, G. E. and Harris, E. G., "Unstable Electrostatic Plasma Waves Propagating Perpendicular to a Magnetic Field", Phys. Rev. Lett. 14, pp. 131-133, Feburary.

Hall, L. S. and Heckrotte, W., "Electrostatic Instabilities of a Plasma with Magnetically Supported Velocity-Space Anisotropy at High Density", Lawrence Livermore Laboratory UCRL-12447, April; Proc. of the Seventh International Conference on Phenomena in Ionized Gases, Vol. II (Beograd, 1966), pp. 624-628.

1966 Mikhailovskii, A. B. and Pashitskii, E. A., "Stability of an Ion Beam Injected into a Plasma Across a Magnetic Field", Sov. Phys. Tech. Phys. 10, pp. 1507-1513, May.

1968 O'Neil, T. M. and Malmberg, J. H., "Transition of the Dispersion Roots from Beam-Type to Landau-Type Solutions", Phys. Fluids 11, pp. 1754-1760, August.

1970 Tataronis, J. A. and Crawford, F. W., "Cyclotron Harmonic Wave Propagation and Instabilities", J. Plasma Phys. 4, pp. 231-264.

1971 Callen, J. D. and Guest, G. E., "Electromagnetic Modifications of the Electrostatic Dispersion Relation", Phys. Fluids 14, pp. 1588-1591, July.

1973 Callen, J. D. and Guest, G. E., "Electromagnetic Effects on Electrostatic Modes in a Magnetized Plasma", Nuclear Fusion 13, pp. 87-110.

1976 Böhmer, H., "Excitation of Ion Cyclotron Harmonic Waves with an Ion Beam of High Perpendicular Energy", Phys. Fluids 19, pp. 1371-1374, September.

Gerver, M. J., Memorandum No. M 77/27, Oct. 31 (University of California, Berkeley; Electronics Research Laboratory); this code, ROOTS is available from the computer of the Lawrence Livermore Laboratory.

Lindgren, N. E., Langdon, A. B. and Birdsall, C. K., "Electrostatic Waves in an Inhomogeneous Collisionless Plasma", Phys. Fluids 19, pp. 1026-1034, July.

Seiler, S., Yamada, M. and Ikezi, H., "Lower Hybrid Instability Driven by a Spiraling Ion Beam", Phys. Rev. Lett. 37, pp. 700-703, September.

1977 Mynick, H. E., Gerver, M. J. and Birdsall, C. K., "Stability Regions and Growth Rates for a Two-Ion Component Plasma, Unmagnetized", Phys. Fluids 20, pp. 606-612, April.

Seiler, S., "Linear and Nonlinear Development of a Lower-Hybrid Wave Driven by a Perpendicular Ion Beam", Ph.D. Thesis, Princeton University.

Yamada, M. and Seiler, S. "Anomalous Slowing of a Perpendicularly Injected Ion Beam in Both Quasilinear and Trapping Regimes", Phys. Rev. Lett. 39, pp. 808-811, September.